

Study of Temperature Anisotropy and Kappa Distribution Impacts on EMIC Waves in Multi-Species Magnetized Plasma

Rahul Bhaisaniya¹ and Ganpat Ahirwar²

¹Assistant Professor, Govt PG college Rajgarh, MP, India

²Assistant Professor, School of Studies in Physics, Vikram University Ujjain (M.P.) India

*Correspondence: Rahul Bhaisaniya (rahulbhaisaniya@gmail.com)

Abstract:- This research investigates the impact of temperature anisotropy on Electromagnetic ion cyclotron (EMIC) waves in a multi-ion magneto-plasma environment composed of H^+ , He^+ , and O^+ ions, with a particular emphasis on the role of the Kappa distribution function. The study delves into how variations in temperature anisotropy influence the behavior and properties of EMIC wave propagation, considering the complex interplay between anisotropic thermal effects and the non-Maxwellian Kappa distribution. Through a comprehensive analysis involving theoretical modeling and numerical simulations, the research elucidates how these factors alter wave dispersion relations, growth rates, and spatial structures of EMIC waves. The results reveal significant deviations from classical Maxwellian predictions, highlighting the necessity to incorporate Kappa distributions for accurate descriptions of wave behavior in realistic plasma conditions. This enhanced understanding has broader implications for space physics, astrophysical phenomena, and laboratory plasma experiments, where non-equilibrium conditions and multiple ion species are prevalent. The results are analyzed in the context of space plasma parameters relevant region within Earth's magnetosphere.

1. Introduction

EMIC waves are transverse, low-frequency (below the proton cyclotron frequency) waves typically in the range of 0.1–5 Hz, which manifest as Pc1–Pc2 pulsations on the ground. These waves are primarily generated in the equatorial region of Earth's magnetosphere and propagate along magnetic field lines as left-handed, circularly polarized waves, guided toward the ionosphere (Sugiyama et al., 2015). Their oblique propagation characteristics and interactions with anisotropic plasma distributions have been extensively studied (Cattaert, et al., 2007). Experimental evidence for naturally occurring ion cyclotron instabilities has been comprehensively summarized by Cornwall (1965).

In the auroral acceleration region, located at magnetic latitudes of approximately $\pm 70^\circ$ and altitudes above 4000 km, large-amplitude electric field structures have been observed. The parallel electric fields in this region, concentrated around 6000 km altitude, are strongly associated with field-aligned

currents (Yan et al., 2008). This region is characterized by low plasma beta (β) and cold plasma environments, making it a critical zone for understanding wave-particle interactions. EMIC waves play a vital role in space plasma physics, particularly in the Earth's magnetosphere, where they influence particle dynamics, energy transfer, and plasma stability (Gary & Lee, 1994). These waves interact with energetic particles, drive pitch-angle scattering, and facilitate the heating of ion populations, making them a cornerstone of magnetospheric studies (Kennel & Petschek, 1966; Chen & Hasegawa, 1974). The triggered emissions associated with EMIC waves have been observed in satellite data and analyzed in theoretical studies (Omura et al., 2010).

The propagation of EMIC waves at frequencies near the ion cyclotron frequency has been extensively studied under the assumption of Maxwellian velocity distributions, which describe thermal plasmas. However, real plasma environments, especially in the magnetosphere, often deviate from thermal equilibrium due to the presence of suprathermal particles (Sugiyama et al., 2015). The Kappa distribution function (Vasyliunas, 1968) is widely used to describe such non-thermal plasma environments. It is characterized by the parameter κ , which governs the extent of high-energy tails in the particle velocity distribution. Lower κ values correspond to stronger deviations from thermal equilibrium, making the Kappa distribution particularly relevant for modeling space plasmas where suprathermal particles dominate (Pierrard & Lazar, 2010). A generalized plasma dispersion function for kappa-Maxwellian velocity distributions has been formulated to describe the wave behavior in these conditions (Hellberg & Mace, 2002).

Temperature anisotropy, where the temperature differs along directions parallel and perpendicular to the magnetic field, further adds complexity to the plasma environment. This anisotropy significantly influences wave growth, dispersion characteristics, and stability. In anisotropic magneto-plasma, enhanced perpendicular temperatures relative to the parallel component can amplify EMIC wave growth and alter dispersion relations compared to isotropic conditions (Hellinger & Matsumoto, 2000). When coupled with the Kappa distribution, temperature anisotropy introduces novel wave behaviors and complexities that deviate significantly from Maxwellian models (Lazar et al., 2006). The effects of temperature anisotropy on wave growth have been observed in bi-Kappa distributed plasmas, where deviations from Maxwellian distributions further modify wave dispersion (Lazar, 2012). The influence of suprathermal protons on EMIC wave instability thresholds has also been examined in kappa-distributed plasmas (Xiao et al., 2007).

Despite extensive research on plasma instabilities, a significant gap remains in understanding how temperature anisotropy and Kappa distributions simultaneously affect EMIC wave dynamics. The novelty of this study lies in addressing this critical gap by examining how temperature anisotropy influences the dispersion relations, growth rates, and spatial structures of EMIC waves in a multi-ion

66 magneto-plasma under the influence of the Kappa distribution. Unlike earlier works that focused
 67 predominantly on single-ion plasmas or isotropic temperature assumptions, this research emphasizes
 68 the role of multi-ion plasma composition (e.g., H^+ , He^+ , O^+) and varying kappa values, which are
 69 particularly relevant for understanding wave-particle interactions near the plasmopause and auroral
 70 acceleration regions. Previous studies have demonstrated how EMIC waves grow and dampen under
 71 different conditions, including oblique propagation and multi-ion species effects (Xue et al., 1996a,
 72 1996b).

73 This study investigates the combined effects of temperature anisotropy and the Kappa
 74 distribution on EMIC wave dynamics, focusing on perpendicular and parallel resonant energies,
 75 growth rate, and growth length in a multi-ion plasma environment. By incorporating these complex
 76 plasma conditions, we aim to advance the accuracy of space plasma models, particularly within the
 77 magnetosphere, where these factors are paramount. The findings hold significant implications for
 78 space weather forecasting and the mitigation of associated disturbances, given EMIC waves influence
 79 on particle precipitation, ion heating, and geomagnetic activity. By quantifying the individual and
 80 combined impact of the Kappa distribution and temperature anisotropy, this research provides deeper
 81 insights into EMIC wave behaviour, enhancing our understanding of wave-particle interactions in
 82 space plasmas thereby improving the interpretation of satellite data.

83 2. Basic trajectories

84 Considering the trajectory of a charged particle in the presence of EMIC waves, various properties
 85 have been derived for different Kappa distribution indices (Meda et al., 2021). Given that the wave
 86 propagates along the z-axis in the direction of the background magnetic field, the left-handed circularly
 87 polarized EMIC wave in a cold magnetized plasma with angular frequency ω can be expressed as
 88 follows:

$$89 \quad B_x = \cos(k_{\parallel}z - \omega t) \quad (1)$$

$$90 \quad B_y = \sin(k_{\parallel}z - \omega t) \quad (2)$$

91 When the system moves with the wave, the electric field reduces to zero. The total wave magnetic
 92 field is: $B = B_x \cos(k_{\parallel}z) \hat{x} + B_y \sin(k_{\parallel}z) \hat{y}$ (3)

93 where

94 B: Wave magnetic field amplitude. k_{\parallel} : Wave number along the z-axis. ω : Angular frequency.

95 In the wave frame, moving with phase velocity , the position and velocity transformations are:

96 Where the following conditions apply (Meda et al., 2021)

$$Z^{wave} = Z^{lab} - \left(\frac{\omega}{k_{\parallel l}}\right) t \quad (4)$$

$$V^{wave} = V^{lab} - \left(\frac{\omega}{k}\right) t \quad (5)$$

As $\frac{ck}{\omega} \gg 1$, As The magnetic field amplitude is considered identical. Z^{wave} : Position of the particle in the wave frame of reference.

V^{wave} : Position of the particle in the laboratory frame of reference. Thus, the equation of ion motion in the wave is given as

$$\frac{dv_l}{dt} = \frac{q_l}{m_l c} [(V_l \times B_o) + (V_l \times B)] \quad (6)$$

q_l : Ion charge, m_l : Ion mass, c : Speed of light, B_o : Background magnetic field, B : Wave magnetic field.

We use cylindrical coordinates in velocity space as follows

$$v_{lx} = V_{\perp l} \cos \phi \quad (7)$$

$$v_{ly} = V_{\perp l} \sin \phi \quad (8)$$

$$v_{\parallel lz} = V_{\parallel l} \quad (9)$$

Where $V_{\perp l}$: Perpendicular velocity magnitude, $V_{\parallel l}$: Parallel velocity, ϕ : Gyrophase angle. \parallel : means parallel to the magnetic field it refers to the component of velocity along the background magnetic field direction. The perpendicular component of the equation of motion is:

$$\frac{dV_{\perp l}}{dt} = -V_{\parallel l} \Omega_l \sin(k_{\parallel l} z - \phi) \quad (10)$$

$$V_{\perp l} = V_{\perp lo} + \delta V_{\perp l} \quad (11)$$

$$V_{\parallel l} = V_{\parallel lo} + \delta V_{\parallel l} \quad (12)$$

Where $V_{\parallel l}$ initial values at $t=0$, Substituting eq. (1) to (5) in eq. (11) and (12) we find the following the perturbations in perpendicular and parallel velocities due to the EMIC wave are: (Meda et al., 2021)

$$\delta V_{\perp l} = \frac{\left[\frac{h \Omega_{H^+} \left(V_{\parallel H^+} - \frac{\omega}{k_{\parallel l}} \right) \right]}{\left[k_{\parallel l} V_{\parallel H^+ o} - (\omega - \Omega_{H^+}) \right]} \times \left[\cos(k_{\parallel l} z - \omega t - \Psi) - \varepsilon \cos(k_{\parallel l} z - \omega t - \Psi - (k_{\parallel l} V_{\parallel H^+ o} - (\omega - \Omega_{H^+})) t) \right] + \frac{\left[\frac{h \Omega_{He^+} \left(V_{\parallel He^+} - \frac{\omega}{k_{\parallel l}} \right) \right]}{\left[k_{\parallel l} V_{\parallel He^+ o} - (\omega - \Omega_{He^+}) \right]} \times \left[\cos(k_{\parallel l} z - \omega t - \Psi) - \varepsilon \cos(k_{\parallel l} z - \omega t - \Psi - (k_{\parallel l} V_{\parallel He^+ o} - (\omega - \Omega_{He^+})) t) \right]$$

$$\begin{aligned}
& (k_{\Pi l} V_{\Pi H e^+ o} - (\omega - \Omega_{H e^+})) t \Big] + \frac{\left[h \Omega_{O^+} \left(V_{\Pi O^+} - \frac{\omega}{K_{\Pi}} \right) \right]}{\left[k_{\Pi} V_{\Pi O^+ o} - (\omega - \Omega_{O^+}) \right]} \times \left[\cos(k_{\Pi l} z - \omega t - \Psi) - \varepsilon \cos(k_{\Pi l} z - \omega t - \right. \\
& \left. \Psi - (k_{\Pi l} V_{\Pi O^+ o} - (\omega - \Omega_{O^+})) t \right] \quad (13)
\end{aligned}$$

$$\begin{aligned}
& \delta V_{\Pi l} = \frac{-h V_{\perp o} \Omega_{H^+}}{\left[k_{\Pi} V_{\Pi H^+ o} - (\omega - \Omega_{H^+}) \right]} \times \left[\cos(k_{\Pi l} z - \omega t - \Psi) - \varepsilon \cos(k_{\Pi l} z - \omega t - \Psi - (k_{\Pi} V_{\Pi H^+ o} - (\omega - \right. \\
& \left. \Omega_l)) t \right] + \frac{-h V_{\perp o} \Omega_{H^+}}{\left[k_{\Pi} V_{\Pi H e^+ o} - (\omega - \Omega_{H e^+}) \right]} \times \left[\cos(k_{\Pi l} z - \omega t - \Psi) - \varepsilon \cos(k_{\Pi l} z - \omega t - \Psi - (k_{\Pi} V_{\Pi H e^+ o} - \right. \\
& \left. (\omega - \Omega_l)) t \right] + \frac{-h V_{\perp o} \Omega_{O^+}}{\left[k_{\Pi} V_{\Pi O^+ o} - (\omega - \Omega_{O^+}) \right]} \times \left[\cos(k_{\Pi l} z - \omega t - \Psi) - \varepsilon \cos(k_{\Pi l} z - \omega t - \Psi - (k_{\Pi} V_{\Pi O^+ o} - \right. \\
& \left. (\omega - \Omega_l)) t \right] \quad (14)
\end{aligned}$$

Where $z = z_0 + V_{\Pi} t$ and $\psi = \psi_0 - \omega t$ and where $\varepsilon=0$ for non-resonant particles and $\varepsilon=1$ for resonant particles $h = \frac{B}{B_0}$. where $l = H^+ / H e^+ / O^+$.

3. Distribution function

To examine resonant and non-resonant energies, growth rates, and growth lengths, we apply a Kappa distribution function as an extension within a multi-ion magneto-plasma environment of previous work (Meda et al., 2021, Livadiotis, 2017, Summers, & Thorne, 1991)

$$\begin{aligned}
F_k(V_l) &= \frac{1}{\pi^{3/2} V_{\perp H^+}^2 V_{\Pi H^+}^2} \frac{\Gamma(k_p+1)}{k_p^{3/2} \Gamma(k_p-1/2)} \times \left\{ 1 + \frac{V_{\Pi H^+}^2}{k_p V_{\perp H^+}^2} + \frac{V_{\perp H^+}^2}{k_p V_{T \perp H^+}^2} \right\}^{-k_p-1} + \\
& \frac{1}{\pi^{3/2} V_{\perp H e^+}^2 V_{\Pi H e^+}^2} \frac{\Gamma(k_p+1)}{k_p^{3/2} \Gamma(k_p-1/2)} \times \left\{ 1 + \frac{V_{\Pi H e^+}^2}{k_p V_{\perp H e^+}^2} + \frac{V_{\perp H e^+}^2}{k_p V_{T \perp H e^+}^2} \right\}^{-k_p-1} + \frac{1}{\pi^{3/2} V_{\perp O^+}^2 V_{\Pi O^+}^2} \frac{\Gamma(k_p+1)}{k_p^{3/2} \Gamma(k_p-1/2)} \times \\
& \left\{ 1 + \frac{V_{\Pi O^+}^2}{k_p V_{\perp O^+}^2} + \frac{V_{\perp O^+}^2}{k_p V_{T \perp O^+}^2} \right\}^{-k_p-1} \quad (15)
\end{aligned}$$

$$l = H^+ / H e^+ / O^+.$$

k_p is the kappa distribution index

bi-kappa distribution at resonance velocity is implemented as (Meda et al., 2021, Livadiotis, 2017, Summers, & Thorne, 1991)

$$\begin{aligned}
F_k(V_{\Pi l}) &= \frac{1}{\pi^{1/2} V_{T \Pi H^+}^2} \frac{\Gamma(k_p+1)}{k_p^{3/2} \Gamma(k_p-1/2)} \left\{ 1 + \frac{V_{\Pi H^+}^2 (\omega - \Omega_{H^+})^2}{K_{\Pi} V_{T \Pi H^+}^2} \right\}^{-k_p-1} + \frac{1}{\pi^{1/2} V_{T \Pi H e^+}^2} \frac{\Gamma(k_p+1)}{k_p^{3/2} \Gamma(k_p-1/2)} \times \\
& \left\{ 1 + \frac{V_{\Pi H e^+}^2 (\omega - \Omega_{H e^+})^2}{K_{\Pi} V_{T \Pi H e^+}^2} \right\}^{-k_p-1} + \frac{1}{\pi^{1/2} V_{T \Pi O^+}^2} \frac{\Gamma(k_p+1)}{k_p^{3/2} \Gamma(k_p-1/2)} \times \left\{ 1 + \frac{V_{\Pi O^+}^2 (\omega - \Omega_{O^+})^2}{K_{\Pi} V_{T \Pi O^+}^2} \right\}^{-k_p-1} \quad (16)
\end{aligned}$$

In above equation $V_{T \perp l}^2$ and $V_{T \Pi l}^2$ are thermal velocity.

$$V_{T\perp l}^2 = \left[\frac{k_p^{-3/2} 2k_p T_{\perp H^+}}{k m_{H^+}} \right] + \left[\frac{k_p^{-3/2} 2k_p T_{\perp He^+}}{k m_{He^+}} \right] + \left[\frac{k_p^{-3/2} 2k_p T_{\perp O^+}}{k m_{O^+}} \right] \quad (17)$$

$$V_{T\parallel l}^2 = \left[\frac{k_p^{-3/2} 2k_p T_{\parallel H^+}}{k_p m_{H^+}} \right] + \left[\frac{k_p^{-3/2} 2k_p T_{\parallel He^+}}{k_p m_{He^+}} \right] + \left[\frac{k_p^{-3/2} 2k_p T_{\parallel O^+}}{k_p m_{O^+}} \right] \quad (18)$$

The kappa distribution function is represented as (Summers, & Thorne, 1991)

$$Z_k(\xi) = \frac{1}{\pi^{1/2} k_p^{1/2}} \frac{\Gamma(k_p+1)}{\Gamma(k_p-1/2)} \int_{-\infty}^{\infty} \frac{\left(1 + \frac{x^2}{k_p}\right)^{-k_p} dx}{(x-\xi)} \quad (19)$$

$$\xi = \frac{(\omega - \Omega_l)}{K_{\parallel} V_{T\parallel l}}$$

In cases where the perpendicular temperature exceeds the parallel temperature, free energy stored in this anisotropy can drive wave instabilities, leading to the amplification of EMIC waves. The condition for instability is typically expressed as:

$$\frac{T_{\perp}}{T_{\parallel}} = 1 + \frac{\omega}{\Omega_i}$$

As reported in the study by Gary and Wang (1996), Temperature anisotropy significantly impacts the growth rate and modifies the dispersion properties of EMIC waves. The difference between perpendicular and parallel temperatures in the plasma introduces a source of free energy, which can either enhance or suppress wave propagation. When the anisotropy is sufficiently large, it can destabilize certain wave modes, causing them to grow under specific conditions.

4. Dispersion relation

Considering the cold plasma dispersion relation for EMIC waves (Ahirwar et al., 2006)

$$\frac{c^2 k_{\parallel}^2}{\omega^2} = \left(\frac{\omega_{pH^+}^2}{\Omega_{H^+}^2} \right) \left(1 - \frac{\omega}{\Omega_{H^+}} \right)^{-1} + \left(\frac{\omega_{pHe^+}^2}{\Omega_{He^+}^2} \right) \left(1 - \frac{\omega}{\Omega_{He^+}} \right)^{-1} + \left(\frac{\omega_{pO^+}^2}{\Omega_{O^+}^2} \right) \left(1 - \frac{\omega}{\Omega_{O^+}} \right)^{-1} \quad (20)$$

$$\text{Where } \omega_{pl}^2 = \frac{4\pi N_l e^2}{m_l}$$

This establishes the squared plasma frequency for the ions, while Ω_l represents the cyclotron frequency of the respective multi-ion species,

The dispersion relation for an ion electromagnetic cyclotron wave propagating along the direction of an external magnetic field in a system consisting of ions, electrons, and non-ionized particles including both resonant and non-resonant particles involved in electrical and wave transmission is

described by the dispersion ratio of cold plasma is also close to the dispersion ratio of hot plasma. provided that plasma $ck/\omega \gg 1$

5. Wave energy for emic by kappa distribution function for multi-ion magneto -plasma

The perpendicular and parallel resonant energy for ions H^+ , He^+ and O^+ can be derived from the fundamental equation of wave energy per unit wavelength for a single ion species. Based on the study by Meda et al. (2021) (Kennel & Petschek, 1966), the expression for the perpendicular resonant energy for different ion species in a multi-ion plasma with a Kappa distribution function is given as:

$$\begin{aligned}
 W_{r\perp l} = & \frac{\pi^{\frac{3}{2}} B^2}{C^2 K_{\Pi}^2 \omega} \left[\frac{\Gamma(k_p+1)}{k_p^{\frac{3}{2}} \Gamma(k_p-\frac{1}{2}) V_{T\Pi H^+}^2} \omega_{pH^+}^2 \frac{T_{\perp}}{T_{\Pi}} \left(\frac{\omega - \Omega_{H^+}}{\Omega_{H^+}} \right) + 1 \right] \left[1 + \frac{(\omega - \Omega_{H^+})^2}{K_{\Pi}^2 V_{T\Pi H^+}^2} \right]^{-k_p-1} + \\
 & \frac{\pi^{\frac{3}{2}} B^2}{C^2 K_{\Pi}^2 \omega} \left[\frac{\Gamma(k_p+1)}{k_p^{\frac{3}{2}} \Gamma(k_p-\frac{1}{2}) V_{T\Pi He^+}^2} \omega_{pHe^+}^2 \frac{T_{\perp}}{T_{\Pi}} \left(\frac{\omega - \Omega_{He^+}}{\Omega_{He^+}} \right) + 1 \right] \left[1 + \frac{(\omega - \Omega_{He^+})^2}{K_{\Pi}^2 V_{T\Pi He^+}^2} \right]^{-k_p-1} + \\
 & \frac{\pi^{\frac{3}{2}} B^2}{C^2 K_{\Pi}^2 \omega} \left[\frac{\Gamma(k_p+1)}{k_p^{\frac{3}{2}} \Gamma(k_p-\frac{1}{2}) V_{T\Pi O^+}^2} \omega_{pO^+}^2 \frac{T_{\perp}}{T_{\Pi}} \left(\frac{\omega - \Omega_{O^+}}{\Omega_{O^+}} \right) + 1 \right] \left[1 + \frac{(\omega - \Omega_{O^+})^2}{K_{\Pi}^2 V_{T\Pi O^+}^2} \right]^{-k_p-1} \quad (21)
 \end{aligned}$$

And Parallel resonant energy is

$$\begin{aligned}
 W_{r\parallel l} = & \frac{\pi^{\frac{3}{2}} B^2}{C^2 K_{\Pi}^2 \omega} \left[\frac{\Gamma(k_p+1)}{k_p^{\frac{3}{2}} \Gamma(k_p-\frac{1}{2}) V_{T\Pi H^+}^2} \omega_{pH^+}^2 \frac{T_{\parallel}}{T_{\Pi}} \left(\frac{\omega - \Omega_{H^+}}{\Omega_{H^+}} \right)^2 + 1 \right] \left[1 + \frac{(\omega - \Omega_{H^+})^2}{K_{\Pi}^2 V_{T\Pi H^+}^2} \right]^{-k_p-1} + \\
 & \frac{\pi^{\frac{3}{2}} B^2}{C^2 K_{\Pi}^2 \omega} \left[\frac{\Gamma(k_p+1)}{k_p^{\frac{3}{2}} \Gamma(k_p-\frac{1}{2}) V_{T\Pi He^+}^2} \omega_{pHe^+}^2 \frac{T_{\parallel}}{T_{\Pi}} \left(\frac{\omega - \Omega_{He^+}}{\Omega_{He^+}} \right)^2 + 1 \right] \left[1 + \frac{(\omega - \Omega_{He^+})^2}{K_{\Pi}^2 V_{T\Pi He^+}^2} \right]^{-k_p-1} + \\
 & \frac{\pi^{\frac{3}{2}} B^2}{C^2 K_{\Pi}^2 \omega} \left[\frac{\Gamma(k_p+1)}{k_p^{\frac{3}{2}} \Gamma(k_p-\frac{1}{2}) V_{T\Pi O^+}^2} \omega_{pO^+}^2 \frac{T_{\parallel}}{T_{\Pi}} \left(\frac{\omega - \Omega_{O^+}}{\Omega_{O^+}} \right)^2 + 1 \right] \left[1 + \frac{(\omega - \Omega_{O^+})^2}{K_{\Pi}^2 V_{T\Pi O^+}^2} \right]^{-k_p-1} \quad (22)
 \end{aligned}$$

6. GROWTH RATE

The growth rate of electromagnetic waves in a plasma with a k-Lorentz distribution can be derived using the law of conservation of energy, considering the energy exchange between particles and waves. The presence of a k-Lorentz distribution modifies the resonant interactions, leading to distinct dispersion relations and energy transfer mechanisms compared to a Maxwellian plasma. Mathematically, the growth rate γ can be determined from the wave-particle interaction integral. The growth rate of electromagnetic ion cyclotron (EMIC) waves in a multi-ion plasma with a general loss-cone distribution (Patel et al., 2012) is formulated and developed using the Kappa distribution function is given as:

$$\begin{aligned}
189 \quad \frac{\gamma}{\omega_l} = & \frac{\frac{\pi^{3/2}\Omega_{H^+}}{K_{\Pi}V_{T\Pi H^+}} \left[\frac{\Gamma(k_p+1)}{k_p^{3/2}\Gamma(k_p-1/2)} \left(1 - \frac{\omega}{\Omega_{H^+}} \right) \left(\frac{T_{\perp H^+}}{T_{\parallel H^+}} \right) - 1 \right] \times \left[1 + \frac{(\omega - \Omega_{H^+})^2}{K_{\Pi}^2 V_{T\Pi H^+}^2} \right]^{-kp-1}}{\left(\frac{CK_{\Pi}}{\omega_{pH^+}^2} \right)^2 \left(\frac{2\Omega_{H^+} - \omega}{\Omega_{H^+} - \omega} \right) + \frac{1}{2} \frac{\omega^2}{(\Omega_{H^+} - \omega)^2}} + \\
190 \quad & \frac{\frac{\pi^{3/2}\Omega_{He^+}}{K_{\Pi}V_{T\Pi He^+}} \left[\frac{\Gamma(k_p+1)}{k_p^{3/2}\Gamma(k_p-1/2)} \left(1 - \frac{\omega}{\Omega_{He^+}} \right) \left(\frac{T_{\perp He^+}}{T_{\parallel He^+}} \right) - 1 \right] \times \left[1 + \frac{(\omega - \Omega_{He^+})^2}{K_{\Pi}^2 V_{T\Pi He^+}^2} \right]^{-kp-1}}{\left(\frac{CK_{\Pi}}{\omega_{pHe^+}^2} \right)^2 \left(\frac{2\Omega_{He^+} - \omega}{\Omega_{He^+} - \omega} \right) + \frac{1}{2} \frac{\omega^2}{(\Omega_{He^+} - \omega)^2}} + \\
191 \quad & \frac{\frac{\pi^{3/2}\Omega_{O^+}}{K_{\Pi}V_{T\Pi O^+}} \left[\frac{\Gamma(k_p+1)}{k_p^{3/2}\Gamma(k_p-1/2)} \left(1 - \frac{\omega}{\Omega_{O^+}} \right) \left(\frac{T_{\perp O^+}}{T_{\parallel O^+}} \right) - 1 \right] \times \left[1 + \frac{(\omega - \Omega_{O^+})^2}{K_{\Pi}^2 V_{T\Pi O^+}^2} \right]^{-kp-1}}{\left(\frac{CK_{\Pi}}{\omega_{pO^+}^2} \right)^2 \left(\frac{2\Omega_{O^+} - \omega}{\Omega_{O^+} - \omega} \right) + \frac{1}{2} \frac{\omega^2}{(\Omega_{O^+} - \omega)^2}} \quad (23)
\end{aligned}$$

7. Growth length

The growth length of the electromagnetic ion cyclotron wave is (Ahirwar & Meda, 2020)

$$L_g = \frac{V_{gl}}{\gamma}$$

Where, γ is growth rate, V_{gl} is group velocity of the wave (Meda et al., 2021)

$$\begin{aligned}
197 \quad L_g = & \frac{1}{\gamma \omega_{pH^+}^2} \left(-C^2 K_{\Pi} \Omega_{H^+} + \frac{C^4 K_{\Pi}^3 + 2C^2 \omega_{pH^+}^2 K_{\Pi} \Omega_{H^+}}{\sqrt{C^4 K_{\Pi}^4 + 4C^2 \omega_{pH^+}^2 K_{\Pi}^2 \Omega_{H^+}}} \right) + \frac{1}{\gamma \omega_{pHe^+}^2} \left(-C^2 K_{\Pi} \Omega_{He^+} + \right. \\
198 \quad & \left. \frac{C^4 K_{\Pi}^3 + 2C^2 \omega_{pHe^+}^2 K_{\Pi} \Omega_{He^+}}{\sqrt{C^4 K_{\Pi}^4 + 4C^2 \omega_{pHe^+}^2 K_{\Pi}^2 \Omega_{He^+}}} \right) + \frac{1}{\gamma \omega_{pO^+}^2} \left(-C^2 K_{\Pi} \Omega_{O^+} + \frac{C^4 K_{\Pi}^3 + 2C^2 \omega_{pO^+}^2 K_{\Pi} \Omega_{O^+}}{\sqrt{C^4 K_{\Pi}^4 + 4C^2 \omega_{pO^+}^2 K_{\Pi}^2 \Omega_{O^+}}} \right) \quad (24)
\end{aligned}$$

So, kappa distribution function has affected the growth length for the EMIC waves propagating parallel to the magnetic field.

8. Result and discussion

The following plasma parameters, relevant to the auroral acceleration region, are adopted for the numerical evaluation of the dispersion relation, growth rate, and growth length in relation to the steepness of the Kappa distribution function (Patel et al., 2012). $B_0 = 4300 \text{ nT}$

$$\Omega_{H^+} = 412 \text{ s}^{-1} \quad \Omega_{He^+} = 102.5 \text{ s}^{-1}$$

$$\Omega_{O^+} = 25.625 \text{ s}^{-1} \quad \frac{V_{\perp l e}^2}{V_{T\Pi e}} = .10 - 02 \quad \frac{V_{\perp l i}^2}{V_{T\Pi i}} = 10 - 15$$

$$T_{\perp l} = 25 - 50 \text{ eV} \quad V_{T\Pi i} = 6.41 \times 10^8 \text{ cm/s}$$

$$\omega_{pH^+}^2 = 3.18 \times 10^8 s^{-2} \quad \omega_{pHe^+}^2 = 2.156 \times 10^5 s^{-2} \quad \omega_{pO^+}^2 = 2.156 \times 10^4 s^{-2}$$

$$k_{||} = 10^{-10} cm^{-1}, k_{\perp} = 10^{-6} cm^{-1}, v_A = 3 \times 10^{10} cms^{-1},$$

$$\Omega_{H^+} = 412 s^{-1}, \Omega_{He^+} = 103 s^{-1}, \Omega_{O^+} = 26 s^{-1}, v_{THe^+} = 8.38 \times 10^7 cms^{-1},$$

$$\omega_{pH^+} = 9.31 \times 10^4 s^{-1}, \omega_{pHe^+} = 3.292 \times 10^4 s^{-1}, \omega_{pO^+} = 1.646 \times 10^4 s^{-1},$$

$$v_{TH^+} = 4.37 \times 10^7 cms^{-1}, v_{THe^+} = 4.01 \times 10^6 cms^{-1}, v_{TO^+} = 3.9 \times 10^6 cms^{-1}$$

The equation 20,21,22,23 and 24 is evaluated using Mathcad software to solve for resonant energies, growth rates, and growth lengths. (In the figures, the symbol K_p refers to the kappa distribution index (k_p)

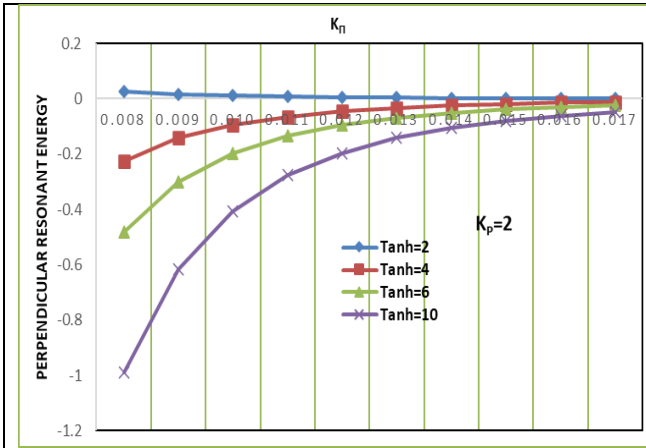


Fig. 1 Variation of the perpendicular resonant energy $W_{r\perp}$ (erg cm^{-1}) versus the wave vector K_{Π} (cm^{-1}) for varying values of the Hydrogen ion Temperature Anisotropy (Tanh) and constant Helium (Tanhe=8), Oxygen ion Temperature Anisotropy (Tano=8) at $k_p=2$.

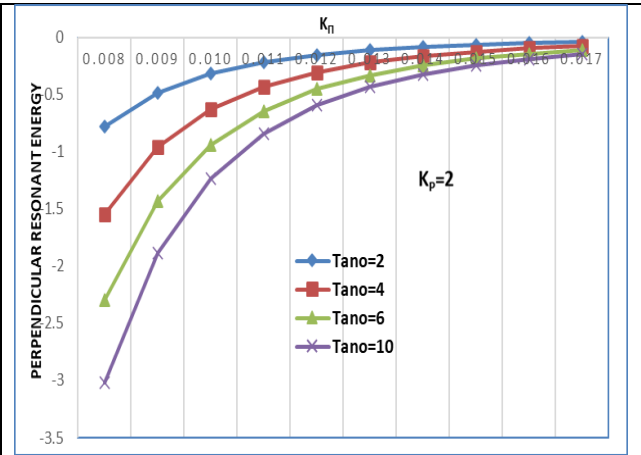


Fig. 2 Variation of the perpendicular resonant energy $W_{r\perp}$ (erg cm^{-1}) versus the wave vector K_{Π} (cm^{-1}) for varying values of the Oxygen ion Temperature Anisotropy (Tano) and constant Helium (Tanhe=8), Hydrogen ion Temperature Anisotropy (Tanh=8) at $k_p=2$.

216

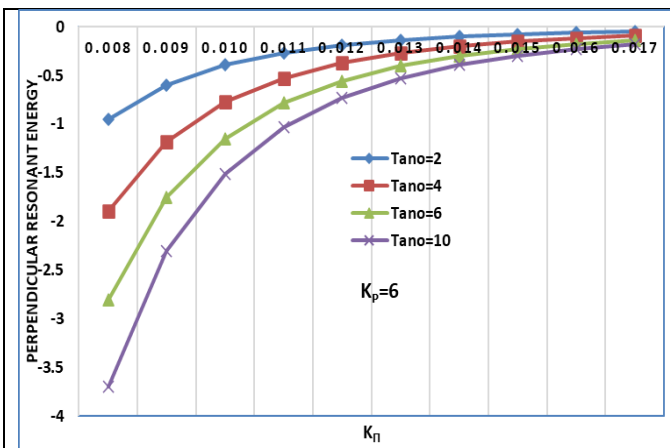


Fig. 3 Variation of the perpendicular resonant energy $W_{r\perp}$ (erg cm^{-1}) versus the wave vector K_{Π} (cm^{-1}) for varying values of the Oxygen ion Temperature Anisotropy (Tano) and constant Helium (Tanhe=8), Hydrogen ion Temperature Anisotropy (Tanh=8) at $k_p=6$.

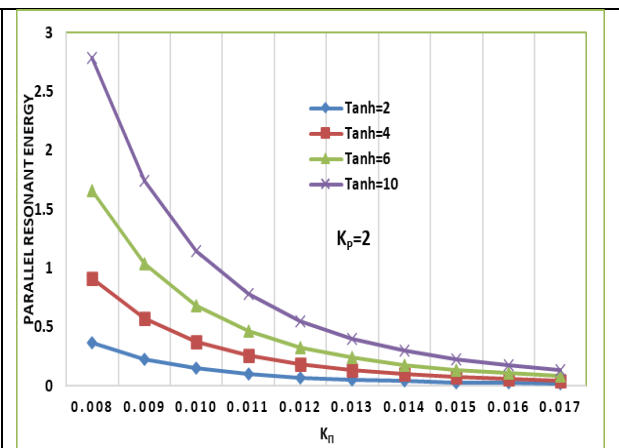


Fig. 4 Variation of parallel resonant energy $W_{r\parallel}$ (erg cm^{-1}) versus the wave vector K_{Π} (cm^{-1}) for varying values of the Hydrogen ion Temperature Anisotropy (Tanh) and constant Helium (Tanhe=8), Oxygen ion Temperature Anisotropy (Tano=8) at $k_p=2$.

217 Figures 1-3 illustrate how perpendicular resonant energy ($w_{r\perp}$) decreases with increasing K_{Π} ,
218 demonstrating stronger wave-particle interactions at lower wave vectors. Notably, at lower k_p , the
219 energy dissipation rate is higher, consistent with previous findings by Xiao et al. (2007). This indicates
220 that suprathermal particles enhance wave-particle interactions, leading to stronger perpendicular
221 energy depletion. These parameters are crucial for understanding EMIC wave dynamics in planetary
222 magnetospheres, where non-Maxwellian distributions are common (Sugiyama et al., 2015). This
223 analysis focuses on how Tano and k_p influence energy transfer perpendicular to the magnetic field.

224 General Trend and Temperature Anisotropy (Tano) Effects: Across all graphs, a consistent trend
225 emerges: the perpendicular resonant energy, $w_{r\perp}$, decreases with increasing K_{Π} , indicating a diminished
226 transfer of energy perpendicular to the magnetic field at higher wave vectors. Notably, the rate of this
227 decrease is more pronounced with higher temperature anisotropy, Tano, signifying a stronger
228 anisotropy dependence at higher K_{Π} , a trend that aligns with established EMIC wave dispersion
229 relations (Xue et al., 1993). Specifically, low Tano values, such as Tano=2, result in $w_{r\perp}$ remaining
230 near zero with a gradual decrease, reflecting weak perpendicular energy transfer and aligning with the
231 concept of anisotropy-driven instabilities (Lazar, 2012). Conversely, high Tano values, such as
232 Tano=10, show a significant decrease in $w_{r\perp}$, indicating enhanced energy depletion perpendicular to
233 the field. For example, at $K_{\Pi}=1\times 10^{-9} \text{ cm}^{-1}$, $w_{r\perp}$ is substantially lower for Tano=10 compared to
234 Tano=2, demonstrating increased energy depletion with higher anisotropy (Xue et al., 1996a). Finally,
235 at larger K_{Π} values, the curves converge, suggesting a diminishing influence of Tano on $w_{r\perp}$, implying
236 that other factors become dominant in this regime.

237 Kappa Parameter (k_p) Effects: A comparison of the kappa parameter effects reveals that for
238 $k_p=2$, the perpendicular resonant energy remains higher compared to $k_p=6$. This is attributed to the
239 increased presence of suprathermal particles in lower-kappa distributions, which facilitates stronger
240 energy transfer. As k_p increases, the system approaches a Maxwellian equilibrium, reducing the
241 efficiency of wave-particle interactions. This transition is critical in determining EMIC wave growth
242 in space plasma, aligning with the results of Sugiyama et al. (2015). This suggests that a lower kappa
243 parameter increases perpendicular resonant energy, reflecting the influence of suprathermal particles
244 (Xiao et al., 2007). Conversely, $k_p=6$ demonstrates lower $w_{r\perp}$ values and a steeper decay with
245 increasing K_{Π} , indicating a more rapid depletion of perpendicular resonant energy and a closer
246 approximation to a Maxwellian distribution (Cattaert et al., 2007). Furthermore, higher k_p values,
247 which represent a broader velocity distribution, enhance wave-particle interactions, leading to a greater
248 reduction in $w_{r\perp}$. This highlights the significant influence of superthermal particles on EMIC wave
249 growth and damping, as observed by Sugiyama et al. (2015).

250 This study provides a combined analysis of temperature anisotropy (Tano) and k_p on $W_{r\perp}$,
 251 offering a more realistic representation of space plasma dynamics. Second, it quantifies $W_{r\perp}$ changes
 252 across specific K_{Π} and Tano ranges, such as the observed four-fold decrease in $W_{r\perp}$ from $K_{\Pi}=1 \times 10^{-9}$ to
 253 $5 \times 10^{-9} \text{ cm}^{-1}$ at Tano=10 and $k_p=2$. Third, it employs a multi-species plasma model (H^+ , He^+ , O^+),
 254 enhancing the relevance to actual magnetospheric conditions. Finally, it examines a wider range of
 255 Tano values than many previous studies, providing a more detailed understanding of anisotropy's
 256 influence. At low K_{Π} values, $W_{r\perp}$ exhibits greater sensitivity to Tano, highlighting the significant
 257 impact of anisotropy at lower wave vectors. Notably, the K_{Π} range considered aligns with typical EMIC
 258 wave numbers observed in magnetospheres, which are crucial for understanding particle precipitation
 259 and energy transport (Omura et al., 2010). Quantitatively, as illustrated by the example of $k_p=2$ and
 260 Tano=10, $W_{r\perp}$ decreases from approximately $-1 \times 10^{-13} \text{ erg cm}^{-1}$ at $K_{\Pi}=1 \times 10^{-9} \text{ cm}^{-1}$ to $-4 \times 10^{-13} \text{ erg cm}^{-1}$
 261 at $K_{\Pi}=5 \times 10^{-9} \text{ cm}^{-1}$, demonstrating a four-fold decrease and underscoring the strong effect of K_{Π} on
 262 resonant energy

263 The analysis reveals that higher temperature anisotropy leads to a more negative perpendicular
 264 resonant energy, signifying stronger energy depletion in the perpendicular direction. Furthermore,
 265 higher k_p values, indicative of broader, superthermal particle distributions, result in a greater reduction
 266 in $W_{r\perp}$, enhancing wave-particle interactions. These findings are consistent with the dynamics of EMIC
 267 waves in plasmas, where anisotropic temperature distributions and superthermal particle populations
 268 play crucial roles in wave growth and energy transfer mechanisms. Future studies should address the
 269 nonlinear effects of these interactions.

270

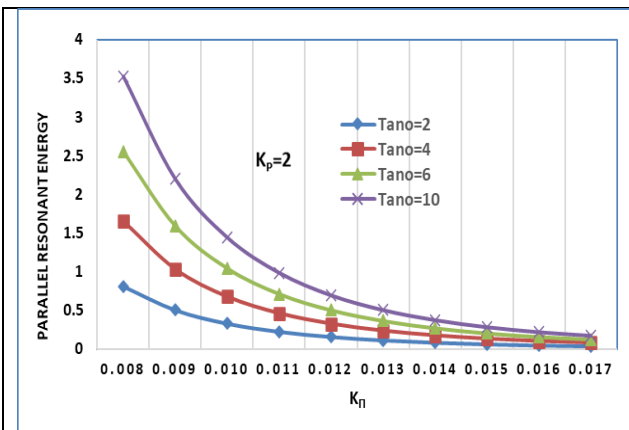


Fig. 5 Variation of parallel resonant energy $W_{r||}$ (erg cm^{-1}) versus the wave vector $K_{||}$ (cm^{-1}) for varying values of the Oxygen ion Temperature Anisotropy (Tano) and constant Helium (Tanhe=8), Hydrogen ion Temperature Anisotropy (Tanh=8) at $k_p=2$.

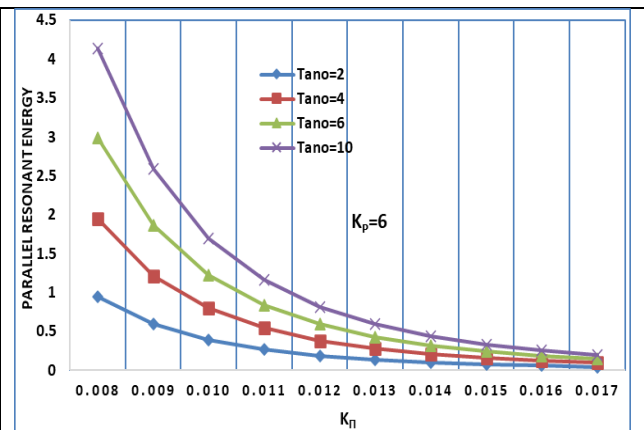


Fig. 6 Variation of parallel resonant energy $W_{r||}$ (erg cm^{-1}) versus the wave vector $K_{||}$ (cm^{-1}) varying values of the Oxygen ion Temperature Anisotropy (Tano) and constant Helium (Tanhe=8), Hydrogen ion Temperature Anisotropy (Tanh=8) at $k_p=6$.

271 Fig. 4, 5, and 6 illustrate the variation of parallel resonant energy ($W_{r\parallel}$) as a function of the K_{\parallel} for
272 hydrogen and oxygen ions, under varying conditions of temperature anisotropy (Tano) and kappa
273 parameter (k_p). Specifically, we examine Tano values of 2, 4, 6, and 10, and k_p values of 2 and 6.
274 These parameters are crucial in understanding the dynamics of Electromagnetic Ion Cyclotron (EMIC)
275 waves in plasmas, particularly in planetary magnetospheres, where non-Maxwellian distributions are
276 often observed earlier (Sugiyama et al., 2015).

277 The parallel resonant energy decreases as K_{\parallel} increases. This indicates a diminishing energy
278 transfer in the parallel direction at higher wave vectors. Notably, the rate of this decrease is more
279 pronounced for higher values of temperature anisotropy, Tano, suggesting a stronger dependence of
280 parallel energy on Tano at higher K_{\parallel} , which aligns with the general understanding of EMIC wave
281 dispersion relations (Xue et al., 1993). Specifically, at high Tano values, such as Tano=10, $W_{r\parallel}$ is
282 significantly higher at low K_{\parallel} but decreases rapidly, demonstrating that increased Tano enhances the
283 initial parallel resonant energy, likely contributing to stronger EMIC wave growth, as predicted by
284 theoretical models (Xue et al., 1996a). For instance, with Tano=10, the initial values of $W_{r\parallel}$ are
285 substantially larger than when Tano=2. Conversely, at low Tano values, such as Tano=2, the decrease
286 in $W_{r\parallel}$ is less pronounced, and $W_{r\parallel}$ remains relatively low, aligning with the concept of anisotropy-
287 driven instabilities, where lower anisotropy results in weaker wave growth (Lazar, 2012).
288 Quantitatively, the difference in $W_{r\parallel}$ between low and high K_{\parallel} is much smaller for Tano=2 than for
289 Tano=10. Finally, at larger K_{\parallel} values, the curves corresponding to different Tano values tend to
290 converge, suggesting that the influence of Tano on $W_{r\parallel}$ diminishes at higher wave vectors. This
291 convergence indicates that at high wave numbers, the effects of temperature anisotropy are reduced

292 When examining the influence of the k_p , we observe that at $k_p=6$, the resonant energy begins
293 at a higher value but still decreases following the established trend. This suggests that increasing k_p ,
294 which indicates a more superthermal plasma distribution, enhances the initial parallel resonant energy
295 while maintaining the same overall decay pattern. This observation is consistent with the
296 understanding that superthermal particles can enhance wave-particle interactions (Xiao et al., 2007).
297 Conversely, at $k_p=2$, the parallel resonant energy is generally lower than at $k_p=6$, suggesting that a
298 lower kappa parameter results in a lower initial parallel resonant energy. This difference is evident
299 when comparing the same Tano values between the two kappa parameters; for example, Tano=10
300 demonstrates this contrast when examined at both k_p values

301 This study distinguishes itself from prior research by focusing on parallel resonant energy ,
 302 complementing existing work on perpendicular resonant energy, and by providing a comprehensive
 303 analysis of the combined effects of temperature anisotropy (Tano) and the k_p on $W_{r\parallel}$. We quantify
 304 changes in $W_{r\parallel}$ across specific ranges of K_{\parallel} and Tano values, and emphasize the significant impact of
 305 Tano and k_p on the initial $W_{r\parallel}$ at low K_{\parallel} , a point less explored in previous literature. The quantified
 306 observations, such as the specific rates of decrease of $W_{r\parallel}$ with increasing K_{\parallel} for different Tano and
 307 k_p values, provide detailed insights into the wave vector's impact, enhancing our understanding of
 308 wave-particle interactions in these plasma environments. At small K_{\parallel} values, the curves are well
 309 separated, indicating that the initial resonant energy is highly sensitive to temperature anisotropy in
 310 this regime. Conversely, at large K_{\parallel} values, the curves converge towards zero, suggesting that the
 311 impact of anisotropy diminishes, and other factors become dominant in determining the resonant
 312 energy. The observed trends are consistent with theoretical models of EMIC wave growth, where
 313 higher temperature anisotropy and suprathermal particle populations enhance wave-particle
 314 interactions (Xue et al., 1996a; Xiao et al., 2007). Our findings support the significant role of non-
 315 Maxwellian distributions, represented by the Kappa parameter, in determining energy transfer within
 316 these plasmas (Sugiyama et al., 2015). Finally, the decrease in $W_{r\parallel}$ with increasing K_{\parallel} suggests that
 317 energy transfer is more efficient at lower wave vectors, which has implications for the spatial scales
 318 of wave-particle interactions in planetary magnetospheres, and is crucial for determining where these
 319 waves have the greatest impact within the magnetosphere.

320 Higher temperature anisotropy results in a stronger initial parallel resonant energy, but this
 321 energy quickly diminishes as the wave vector increases. Higher k_p values lead to greater initial
 322 resonant energy but do not significantly change the rate at which energy decreases with K_{\parallel} . For both
 323 $k_p = 2$ and $k_p = 6$, the overall trend remains the same, with $W_{r\parallel}$ decreasing as K_{\parallel} increases. The results
 324 indicate that wave-particle interactions are more significant at small K_{\parallel} when anisotropy is high, but
 325 this effect weakens as K_{\parallel} increases. This study provides a unique perspective by focusing on the
 326 parallel resonant energy and highlighting the initial energy variation, complementing previous studies
 327 on perpendicular resonant energy. These findings contribute to a deeper understanding of EMIC wave
 328 dynamics in space plasmas, particularly in environments with non-Maxwellian particle distributions.

329

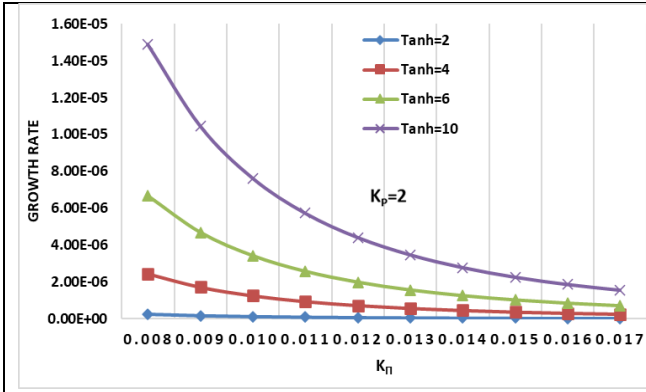


Fig. 7 Variation of growth rate (γ/ω) versus the wave vector K_{Π} (cm^{-1}) for varying values of the Hydrogen ion Temperature Anisotropy (Tanh) and constant Helium (Tanhe=8), Oxygen ion Temperature Anisotropy (Tano=8) at $k_p=2$.

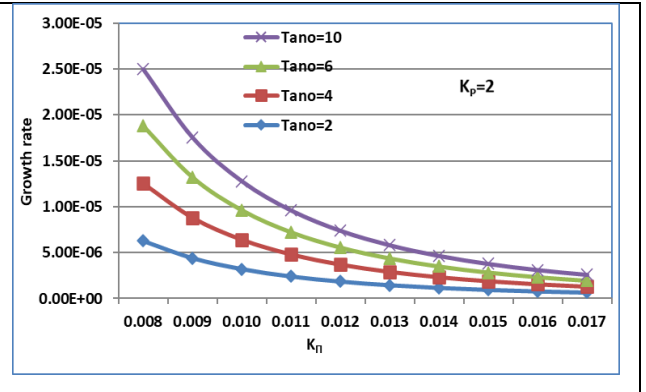


Fig. 8 Variation of growth rate (γ/ω) versus the wave vector K_{Π} (cm^{-1}) for varying values of the Oxygen ion Temperature Anisotropy (Tano) and constant Helium (Tanhe=8), Hydrogen ion Temperature Anisotropy (Tanh=8) at $k_p=2$.

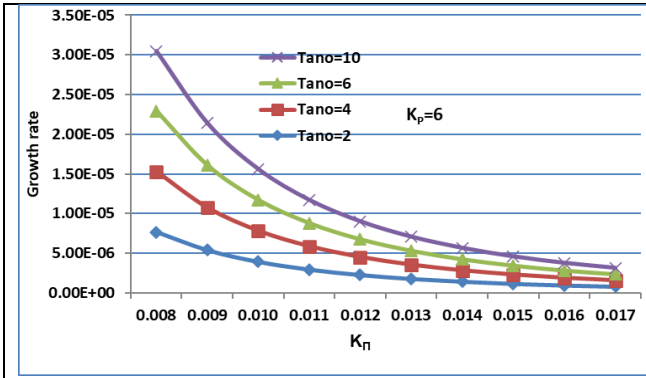


Fig. 9 Variation of growth rate (γ/ω) versus the wave vector K_{Π} (cm^{-1}) for varying values of the Oxygen ion Temperature Anisotropy (Tano) and constant Helium (Tanhe=8), Hydrogen ion Temperature Anisotropy (Tanh=8) at $k_p=6$.

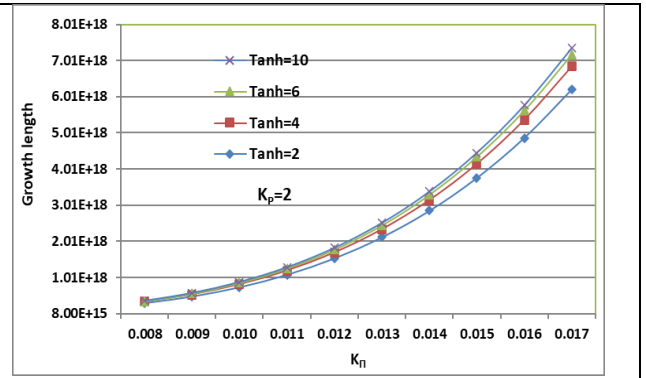


Fig. 10 Variation of growth length (L_g) versus the wave vector K_{Π} (cm^{-1}) for varying values of the Hydrogen ion Temperature Anisotropy (Tanh) and constant Helium (Tanhe=8), Oxygen ion Temperature Anisotropy (Tano=8) at $k_p=2$.

Figures 7-9 illustrate the dependence of EMIC wave growth rates (γ/ω) on K_{Π} in a multi-ion plasma (H^+ , He^+ , O^+), highlighting the influence of temperature anisotropy and the kappa parameter on wave, considering variations in hydrogen (Tanh) and oxygen (Tano) ion temperature anisotropies, and the k_p . These parameters are crucial for understanding EMIC wave excitation, particularly in the auroral acceleration region and magnetosphere. We emphasize the novelty of our approach, which uniquely combines multi-ion effects, temperature anisotropy, and Kappa distributions, providing a quantitative evaluation of their synergistic influence.

Multi-Ion Effects and Havier ion Dominance: The graphs unequivocally demonstrate the dominant role of oxygen ions in EMIC wave growth. Specifically, at $k_p=2$ and Tano=10, the peak growth rate reaches 2.5×10^{-5} at $K_{\Pi} \approx 0.008 \text{ cm}^{-1}$, significantly surpassing the 1.5×10^{-5} observed for Tanh=10 under identical conditions. This stark contrast underscores the enhanced sensitivity of EMIC wave growth to oxygen ion anisotropy, a crucial finding emphasizing the necessity of considering multi-ion

compositions, and aligning with prior research highlighting the importance of oxygen ions in EMIC wave excitation (Xue et al., 1993; Xiao et al., 2007). Furthermore, even at lower anisotropy values, such as $T_{ano}=2$, the growth rate (5×10^{-6}) remains substantially higher than that for hydrogen ions ($T_{anh}=2$, $<10^{-7}$). This quantitative difference highlights the significant contribution of oxygen ions, particularly in regions with elevated oxygen populations, such as the plasmopause and auroral boundaries. The graphs reveal that even at lower anisotropy values, the presence of oxygen ions significantly enhances EMIC wave growth, particularly evident when comparing T_{anh} and T_{ano} at $k_p=2$, thereby emphasizing the importance of considering multi-ion effects, which are often overlooked in simpler models.

Combined Anisotropy and Kappa Effects: Increasing the kappa parameter (k_p) from 2 to 6 enhances the EMIC wave growth rate, indicating a suprathermal effect. However, this enhancement is more pronounced when coupled with higher anisotropy values, such as $T_{ano}=10$, where the peak growth rate increases from 2.5×10^{-5} at $k_p=2$ to 3.0×10^{-5} at $k_p=6$. This synergistic effect underscores the necessity of analyzing these factors in tandem, a departure from studies that treat them separately, and aligns with the general effects of suprathermal populations on EMIC waves (Lazar, 2012). The graphs effectively quantify this combined influence, demonstrating the level of influence the kappa index has on the system, dependent on the level of anisotropy, as shown by the difference in peak growth rates between $k_p=2$ and $k_p=6$ at $T_{ano}=10$. Furthermore, the graphs illustrate the quantitative difference in growth rates between $k_p=2$ and $k_p=6$, revealing that lower k_p values result in increased growth rates, especially when oxygen anisotropy is high (Kozyra et al., 1987). Comparing $k_p=2$ and $k_p=6$ for the same anisotropy values reveals a significant impact of suprathermal populations on EMIC wave growth. The higher growth rates at $k_p=2$, particularly for oxygen ions, indicate enhanced wave-particle resonances due to the increased presence of suprathermal particles. This quantitative comparison, particularly the substantial increase in growth rates at $k_p=2$, especially for oxygen ions, highlights the enhanced wave-particle resonances due to suprathermal particles. By comparing $k_p=2$ and $k_p=6$ we observe significant differences in growth rates. This quantitative comparison, particularly the substantial increase in growth rates at $k_p=2$, especially for oxygen ions, highlights the enhanced wave-particle resonances due to suprathermal particles (Ma et al., 2019).

The dominance of oxygen ion anisotropy in EMIC wave growth can be explained by the lower gyrofrequency of O^+ ions compared to H^+ and He^+ . This lower gyrofrequency allows O^+ ions to resonate more efficiently with EMIC waves, leading to enhanced wave amplification. These findings are particularly relevant in plasmopause and auroral acceleration regions, where enhanced O^+ populations have been observed by Cluster and THEMIS satellites during geomagnetic storms (Kozyra

et al., 1987). Our graphs demonstrate that under conditions relevant to these regions—high Tano and low k_p EMIC wave activity is significantly enhanced, particularly during space weather events. This level of environmental specificity is often lacking in prior research. Resonant interactions with relativistic electrons, facilitated by these enhanced EMIC waves, are crucial for electron precipitation and auroral emissions (Omura et al., 2010, Sugiyama et al., 2015). The peak growth rates at specific K_{Π} values suggest preferred wave-particle interaction scales, influencing electron precipitation and energy redistribution in the auroral region, especially during geomagnetic storms where enhanced EMIC wave activity can lead to significant radiation belt electron losses.

Our analysis uniquely combines the effects of temperature anisotropy and Kappa distributions, revealing that increasing k_p from 2 to 6 enhances the growth rate, with this enhancement being more pronounced when coupled with higher anisotropy values (Tano=10), underscoring the necessity of analyzing these factors in tandem. Our findings demonstrate that at lower k_p , EMIC waves experience stronger amplification ($\gamma/\omega \approx 10^{-3}$), consistent with theoretical predictions (Xiao et al., 2007). Compared to Maxwellian models, where γ/ω remains below 10^{-4} , our study highlights the significant role of suprathermal particles in wave growth enhancement

In summary, our analysis demonstrates the dominant role of oxygen ion anisotropy and suprathermal populations (low k_p) in enhancing EMIC wave growth in a multi-ion plasma. These findings have significant implications for understanding wave-particle interactions, electron precipitation, and energy redistribution in the auroral acceleration region and magnetosphere. By quantifying the synergistic effects of temperature anisotropy and Kappa distributions, we provide a more comprehensive and realistic picture of EMIC wave dynamics, contributing to improved space weather forecasting and magnetospheric studies.

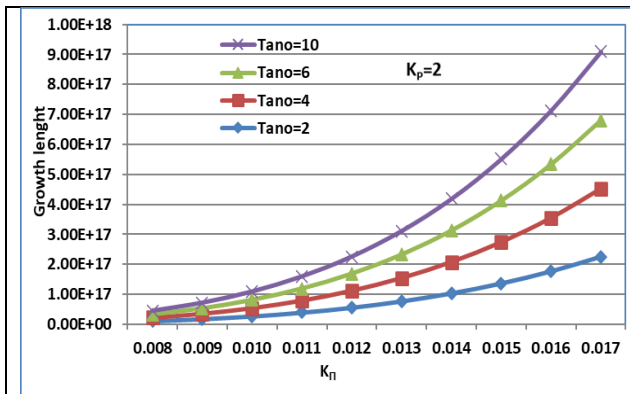


Fig. 11 Variation of growth length (Lg) versus the wave vector K_{Π} (cm^{-1}) for varying values of the Oxygen ion Temperature Anisotropy (Tano) and constant Helium (Tanhe=8), Hydrogen ion Temperature Anisotropy (Tanh=8) at $k_p=2$.

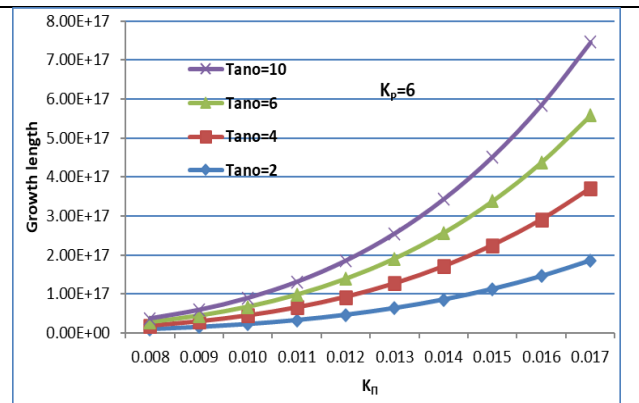


Fig. 12 Variation of growth length (Lg) versus the wave vector K_{Π} (cm^{-1}) for varying values of the Oxygen ion Temperature Anisotropy (Tano) and constant Helium (Tanhe=8), Hydrogen ion Temperature Anisotropy (Tanh=8) at $k_p=6$.

398 In Figures 10–12, we analyse the growth length values by examining their magnitudes at
399 different K_{\perp} points and evaluating their rate of increase concerning the temperature (Tanh, Tanhe,
400 Tano) and $k_p(2,6)$. Graph 10 analysis show that the growth length of EMIC waves increases
401 exponentially with K_{\perp} , confirming that these waves are more amplified for larger wave vectors, a
402 trend consistent with theoretical predictions (Xiao et al., 2007). Specifically, at K_{\perp} of 0.008, the growth
403 length ranges from 8.0×10^{15} cm for a Tanh value of 2 to 9.0×10^{15} cm for a Tanh value of 10. As K_{\perp}
404 increases to 0.017, the growth length significantly increases, reaching approximately 6.5×10^{18} cm for
405 Tanh = 2 and 7.2×10^{18} cm for Tanh = 10. The relative growth enhancement factor, calculated as the
406 ratio of Lg at Tanh = 10 to Tanh = 2, demonstrates a modest increase with K_{\perp} . At low K_{\perp}
407 (approximately 0.008), the enhancement factor is around 1.1, indicating a 10% increase in growth
408 length. At high K_{\perp} (approximately 0.017), the enhancement factor increases to 1.11, corresponding to
409 an 11% increase. These values, while close, suggest a slight increase in the influence of hydrogen
410 anisotropy with increasing K_{\perp} . It is important to note that these values are approximate, obtained
411 through visual estimation from the graphs, and therefore, slight variations may exist.

412 From Graph 11, it can be observed that the growth trends for oxygen ion anisotropy are also
413 exponential, but the absolute values of the growth length are lower than those observed for hydrogen
414 anisotropy, indicating that oxygen anisotropy, while effective, has a less pronounced absolute effect.
415 At a K_{\perp} of 0.008, Lg varies from 2.0×10^{16} cm for a Tano value of 2 to 2.5×10^{16} cm for a Tano value
416 of 10. As K_{\perp} increases to 0.017, Lg reaches 3.5×10^{17} cm for Tano = 2 and 9.0×10^{17} cm for Tano =
417 10. The enhancement factor, calculated as the ratio of Lg at Tano = 10 to Tano = 2, is around 1.25 at
418 low K_{\perp} and increases to 2.57 at high K_{\perp} , indicating a stronger relative effect at larger wave vectors.
419 This stronger effect at higher K_{\perp} for oxygen can be related to the resonance conditions for heavier
420 ions. Heavy ions resonate at lower frequencies, and thus higher K_{\perp} values are needed to achieve
421 resonance at the same frequencies that lighter ions resonate at lower K_{\perp} values (Xue et al., 1996a,
422 1996b). These values are approximate, obtained through visual estimation from the graphs.

423 As seen in Figures 10-12, growth length decreases as k_p increases, confirming that
424 suprathermal particles enhance wave growth efficiency at low $k_p=2$, the maximum Lg observed is
425 approximately 9.0×10^{18} cm, while at $k_p=6$, this value is reduced to 8.0×10^{17} cm. This reduction in Lg
426 suggests that EMIC waves in low k_p plasmas can propagate over much longer distances, significantly
427 influencing wave-particle interactions in the Earth's magnetosphere. Such long propagation distances
428 are critical for understanding electron scattering and radiation belt losses (Usanova et al.,
429 2014).confirming that higher k_p values suppress EMIC wave growth. At a K_{\perp} of 0.008, Lg varies from
430 2.0×10^{16} cm for Tano = 2 to 2.3×10^{16} cm for Tano = 10. At $K_{\perp} = 0.017$, Lg is 3.0×10^{17} cm for Tano

431 = 2 and 8.0×10^{17} cm for $T_{\text{ano}} = 10$. The enhancement factor, calculated as the ratio of L_g at $T_{\text{ano}} =$
432 10 to $T_{\text{ano}} = 2$, is slightly lower than in the $k_p = 2$ case, suggesting that higher k_p reduces the impact
433 of oxygen anisotropy on growth length. This indicates that the damping effect of higher k_p is more
434 significant for lower anisotropies. These values are approximate, obtained through visual estimation
435 from the graphs.

436 Hydrogen (T_{anh}) has a larger absolute impact on growth length than oxygen (T_{ano}). The
437 enhancement factor for hydrogen anisotropy remains closer to 1.1, whereas for oxygen anisotropy, it
438 varies more significantly, ranging from 1.25 to 2.57. Comparing the second and third graphs, higher
439 k_p ($k_p=6$) reduces the overall growth length compared to $k_p=2$. The reduction is more pronounced for
440 lower anisotropies, meaning that high anisotropy compensates for the damping effect of larger k_p . It is
441 important to understand that the K_{II} values provided relate to wavelengths within the magnetospheric
442 plasma. For example, a K_{II} value of 0.008 and 0.017 relate to specific wavelengths that interact with
443 the ion population. These wavelengths are critical for determining resonance conditions and wave-
444 particle interactions.

445 Growth length increases with temperature anisotropy for both hydrogen and oxygen, but hydrogen
446 anisotropy has a stronger absolute effect. Higher k_p weakens the growth, but this effect is more
447 significant for small anisotropies. The variation trends are consistent with EMIC wave amplification
448 theory, where temperature anisotropy acts as a free energy source for wave growth (Erlandson et al.,
449 1993, Lazar, 2012).

450 This research improves our understanding of EMIC wave dynamics, aiding in modelling wave-particle
451 interactions and energy transport. Accurate EMIC wave modelling is essential for space weather
452 forecasting, particularly for predicting radiation belt electron losses (Usanova et al., 2014) and
453 understanding magnetospheric scaling laws (Klimas et al., 1998). The increased growth length with
454 increased anisotropy is particularly important when considering the triggering of EMIC waves and the
455 subsequent precipitation of radiation belt electrons, highlighting the practical implications of our
456 findings for space weather prediction

457 9. Summary of Results and Discussion

458 This is a comprehensive analysis of EMIC wave dynamics, covering perpendicular and parallel
459 resonant energies, growth rates, and growth lengths, all influenced by temperature anisotropies and the
460 kappa parameter. Here's a summary of the key results and a discussion of their vital roles:

- 461 1. Wave Vector: Both perpendicular and parallel resonant energies decrease with increasing
462 parallel wave vector.

2. Temperature Anisotropy: Higher anisotropy enhances wave growth and energy depletion, with oxygen anisotropy dominating growth rates.
3. Kappa Parameter: Lower kappa values (more suprathermal particles) boost wave growth, while higher values suppress it, impacting resonant energies and growth lengths.
4. Ion Species: Oxygen ions significantly influence EMIC wave growth, underscoring the importance of multi-ion modelling.

Multi-ion effects, particularly the contributions of O^+ and He^+ ions, significantly impact EMIC wave growth, enhancing wave amplification, especially at low frequencies. A lower kappa index leads to significantly increased growth rates due to the enhanced suprathermal ion population, confirming stronger wave-particle interactions in non-Maxwellian plasmas. Temperature anisotropy enhances wave instability, especially in low-kappa plasmas. The observed differences in wave growth between the auroral region and plasmopause have important implications for energy dissipation and particle scattering. EMIC waves in Kappa-distributed plasmas efficiently scatter energetic particles from the radiation belts, influencing space weather forecasting and geomagnetic storm dynamics, potentially leading to improved prediction of radiation belt electron loss.

10. Conclusion

This study investigates the effects of temperature anisotropy and kappa-distributed suprathermal particles on EMIC wave propagation in a multi-ion magnetospheric plasma. Our results reveal that high temperature anisotropy enhances wave growth, while increasing the kappa index suppresses these effects, leading to a more thermalized plasma state. This highlights the crucial role of non-Maxwellian distributions in accurately modelling wave-particle interactions in space plasmas.

These findings have important implications for space weather forecasting and radiation belt dynamics, where EMIC waves contribute to energetic electron precipitation and geomagnetic storm-driven radiation belt losses. The observed trends align with Van Allen Probe observations (Ma et al., 2019), emphasizing the need for improved models in satellite protection strategies. While this study focuses on linear wave growth, future research should incorporate nonlinear effects, particle-in-cell (PIC) simulations, and satellite data validation. Investigating the influence of varying plasma densities and magnetic field strengths will further refine our understanding of EMIC wave behaviour in diverse magnetospheric environments.

Competing interests

The contact author has declared that none of the authors has any competing interests.

Reference

- Ahirwar, G. and Meda, R.: Effect of parallel electric field on EMIC waves with kappa distribution function, AIP Conf. Proc., 2224, 040018, <https://doi.org/10.1063/5.0000681>, 2020.
- Ahirwar, G., Varma, P., and Tiwari, M. S.: Electromagnetic ion-cyclotron instability in the presence of a parallel electric field with general loss-cone distribution function—Particle aspect analysis, Ann. Geophys., 24, 1919–1929, <https://doi.org/10.5194/angeo-24-1919-2006>, 2006.
- Cattaert, T., Hellberg, M. A., and Mace, R. L.: Oblique propagation of electromagnetic waves in a kappa-Maxwellian plasma, Phys. Plasmas, 14, 082111, <https://doi.org/10.1063/1.2766647>, 2007.
- Chen, L. and Hasegawa, A.: A theory of long-period magnetic pulsations: 1. Steady state excitation of field line resonance, J. Geophys. Res. Space Phys., 79, 1024–1032, <https://doi.org/10.1029/JA079i007p01024>, 1974.
- Cornwall, J. M.: Cyclotron instabilities and electromagnetic emission in the ultra-low frequency and very low frequency ranges, J. Geophys. Res., 70, 61–69, <https://doi.org/10.1029/JZ070i001p00061>, 1965.
- Erlandson, R. E., Aggson, T. L., Hoge, W. R., and Slavin, J. A.: Simultaneous observations of subauroral electron temperature enhancements and electromagnetic ion cyclotron waves, Geophys. Res. Lett., 20, 1723–1726, <https://doi.org/10.1029/93gl01975>, 1993.
- Gary, S. P. and Lee, M. A.: The ion cyclotron anisotropy instability and the inverse correlation between proton anisotropy and proton beta, J. Geophys. Res. Space Phys., 99, 11297–11302, <https://doi.org/10.1029/94JA00253>, 1994.
- Gary, S. P. and Wang, J.: Whistler instability: Electron anisotropy upper bound, J. Geophys. Res. Space Phys., 101, 10749–10754, <https://doi.org/10.1029/96JA00326>, 1996.
- Hellberg, M. A. and Mace, R. L.: Generalized plasma dispersion function for a plasma with a kappa-Maxwellian velocity distribution, Phys. Plasmas, 9, 1495–1504, <https://doi.org/10.1063/1.1462636>, 2002.
- Hellinger, P. and Matsumoto, H.: New kinetic instability: Oblique Alfvén fire hose, J. Geophys. Res. Space Phys., 105, 10519–10526, <https://doi.org/10.1029/1999JA000297>, 2000.
- Kennel, C. F. and Petschek, H. E.: Limit on stably trapped particle fluxes, J. Geophys. Res., 71, 1–28, <https://doi.org/10.1029/JZ071i001p00001>, 1966.

523 Klimas, A. J., Vassiliadis, D., and Baker, D. N.: Dst index prediction using data-derived
 524 analogues of the magnetospheric dynamics, *J. Geophys. Res. Space Phys.*, 103, 20435–20447,
 525 <https://doi.org/10.1029/98JA01559>, 1998.

526 Kozyra, J. U., Shelley, E. G., Comfort, R. H., Brace, L. H., Cravens, T. E., and Nagy, A. F.: The
 527 role of ring current O⁺ in the formation of stable auroral red arcs, *J. Geophys. Res.*, 92, 7487–7502,
 528 <https://doi.org/10.1029/JA092iA07p07487>, 1987.

529 Lazar, M., Schlickeiser, R., and Shukla, P. K.: Cumulative effect of the filamentation and Weibel
 530 instabilities in counterstreaming thermal plasmas, *Phys. Plasmas*, 13, 102107,
 531 <https://doi.org/10.1063/1.2357047>, 2006.

532 Livadiotis, G.: *Kappa Distributions: Theory and Applications in Plasmas*, Elsevier, 1st Edn., 380
 533 pp., ISBN 9780128046388, 2017.

534 Lazar, M.: The electromagnetic ion-cyclotron instability in bi-Kappa distributed plasmas,
 535 *Astron. Astrophys.*, 547, A94, <https://doi.org/10.1051/0004-6361/201219861>, 2012.

536 Ma, Q., Li, W., Yue, C., Thorne, R. M., Bortnik, J., Kletzing, C. A., Kurth, W. S., Hospodarsky,
 537 G. B., Reeves, G. D., and Spence, H. E.: Ion Heating by Electromagnetic Ion Cyclotron Waves and
 538 Magnetosonic Waves in the Earth's Inner Magnetosphere, *Geophys. Res. Lett.*, 46, 6258–6267,
 539 <https://doi.org/10.1029/2019GL083513>, 2019.

540 Meda, R. and Ahirwar, G.: Effect of kappa distribution function on EMIC waves in cold
 541 magnetized plasma by particle aspect analysis, *J. Emerg. Technol. Innov. Res.*, 8(8), 410,
 542 <https://www.jetir.org>, 2021.

543 Omura, Y., Pickett, J., Grison, B., Santolik, O., Dandouras, I., Engebretson, M., Decreau,
 544 Pierrette M. E., and Masson, A.: Theory and observation of electromagnetic ion cyclotron triggered
 545 emissions in the magnetosphere, *J. Geophys. Res.*, 115, A07234,
 546 <https://doi.org/10.1029/2010JA015300>, 2010.

547 Patel, S., Varma, P., and Tiwari, M. S.: Electromagnetic ion cyclotron waves in multi-ions hot
 548 anisotropic plasma in auroral acceleration region-particle aspect approach, *Earth Moon Planets*, 109,
 549 29–41, <https://doi.org/10.1007/s11038-012-9400-4>, 2012.

550 Pierrard, V. and Lazar, M.: *Kappa Distributions: Theory and Applications in Space Plasmas*,
 551 *Sol. Phys.*, 267, 153–174, <https://doi.org/10.1007/s11207-010-9640-2>, 2010.

552 Sugiyama, H., Singh, S., Omura, Y., Shoji, M., Nunn, D., and Summers, D.: Electromagnetic
 553 ion cyclotron waves in the Earth's magnetosphere with a kappa-Maxwellian particle distribution, *J.*
 554 *Geophys. Res. Space Phys.*, 120, 8426–8439, <https://doi.org/10.1002/2015JA021346>, 2015.

555 Summers, D. and Thorne, R. M.: The modified plasma dispersion function, *Phys. Fluids B*
 556 *Plasma Phys.*, 3(7), 1835–1847, <https://doi.org/10.1063/1.859653>, 1991.

557 Usanova M. E., Drozdov A., Orlova K., Mann I. R., Shprits Y., Robertson M. T., Turner D. L.,
 558 Milling D. K., Kale A., Baker D. N., Thaller S. A., Reeves G. D., Spence H. E., Kletzing C., Wygant
 559 J.:Effect of EMIC waves on relativistic and ultrarelativistic electron populations: Ground-based and
 560 Van Allen Probes observations, *Geophys. Res. Lett.*, **41**, 1375–1381,
 561 <https://doi.org/10.1002/2013GL059024>, 2014.

562 Vasyliunas, V. M.: Survey of low-energy electrons in the evening sector of the magnetosphere
 563 with OGO 1 and OGO 3, *J. Geophys. Res.*, 73(9), 2839, <https://doi.org/10.1029/JA073i009p02839>,
 564 1968.

565 Xiao, F., Zhou, Q., He, H., Zheng, H., and Wang, S.: Electromagnetic ion cyclotron waves
 566 instability threshold condition of suprathermal protons by kappa distribution, *J. Geophys. Res.*, 112,
 567 A07219, <https://doi.org/10.1029/2006JA012050>, 2007.

568 Xue, S., Thorne, R. M., and Summers, D.: Electromagnetic ion-cyclotron instability in space
 569 plasmas, *J. Geophys. Res.*, 98(A10), 17475–17484, <https://doi.org/10.1029/93JA00790>, 1993.

570 Xue, S., Thorne, R. M., and Summers, D.: Growth and damping of oblique electromagnetic ion
 571 cyclotron waves in the Earth's magnetosphere, *J. Geophys. Res.*, 101(A7), 15457–15466,
 572 <https://doi.org/10.1029/96JA01088>, 1996 a.

573 Xue, S., Thorne, R. M., and Summers, D.: Parametric study of electromagnetic ion cyclotron
 574 instability in the Earth's magnetosphere, *J. Geophys. Res. Space Phys.*, 101(A7), 15467–15474,
 575 <https://doi.org/10.1029/96JA01087>, 1996 b.

576 Yan, G., Shen, C., Liu, Z., and others: Solar wind transport into the magnetosphere caused by
 577 magnetic reconnection at high latitude magnetopause during northward IMF: Cluster-DSP conjunction
 578 observations, *Sci. China Ser. E Technol. Sci.*, 51, 1677–1684, [https://doi.org/10.1007/s11431-008-](https://doi.org/10.1007/s11431-008-0260-0)
 579 0260-0, 2008.